Magnetic, electrical, thermal transport, and thermoelectric properties of the ξ' and Ψ complex metallic alloy phases in the Al-Pd-Mn system

J. Dolinšek, P. Jeglič, and P. J. McGuiness
J. Stefan Institute, University of Ljubljana, Jamova 39, SI-1000 Ljubljana, Slovenia

Z. Jagličić
Institute of Mathematics, Physics and Mechanics, Jadranska 19, SI-1000 Ljubljana, Slovenia

A. Bilušić, Ž. Bihar, and A. Smontara
Institute of Physics, Bijenička 46, POB 304, HR-10001 Zagreb, Croatia

C. V. Landauro
Institute for Theoretical Physics, University of Nijmegen, Toernooiveld 1, 6525 ED Nijmegen, The Netherlands

M. Feuerbacher, B. Grushko, and K. Urban
Institut für Festkörperforschung, Forschungszentrum Jülich, Jülich D-52425, Germany
(Received 19 January 2005; published 30 August 2005)

The Al-Pd-Mn system of intermetallics contains complex metallic alloy (CMA) phases, whose crystal structures are based on giant unit cells comprising up to more than a thousand atoms per cell. We performed investigation of the magnetic, electrical, and thermal transport and thermoelectric properties of the ξ' phase and the related Ψ phase on single-crystalline samples grown by the Bridgman technique. The samples are diamagnets with a tiny paramagnetic Curie-like magnetization and an estimated fraction of magnetic Mn atoms about 100 ppm. The electrical resistivity between 300 and 4 K exhibits a temperature variation of less than 2%. The origin of this temperature-compensated resistivity is analyzed in terms of the spectral conductivity model. The thermal conductivity of the samples is small and can be described by the sum of the electronic and lattice contributions, which are of comparable size at room temperature. The lattice contribution can be reproduced by the sum of the Debye term (long-wavelength phonons) and the term due to hopping of localized vibrations. The thermoelectric power is small and negative, compatible with a low concentration of electrons as the majority charge carriers. The studied physical properties of the giant-unit-cell CMA phases in the Al-Pd-Mn system are in many respects intermediate between those of metals or simple intermetallics and quasicrystals, suggesting that both the polytetrahedral local atomic order and the large-scale periodicity influence the physical properties of the material.

DOI: 10.1103/PhysRevB.72.064208 PACS number(s): 61.44.−n, 72.15.−v

I. INTRODUCTION

The term "complex metallic alloys"[1,2] (CMAs) denotes intermetallic phases whose giant unit cells with lattice parameters of several nanometers contain from many tens up to more than a thousand atoms. Examples of CMAs are cubic $NaCd_2$ with 1152 atoms/unit cell,[3,4] the "Bergman phase" $Mg_{32}(Al,Zn)_{49}$ (162 atoms/u.c.),[5] β-Al_3Mg_2 (1168 atoms/u.c.),[6,7] λ-Al_4Mn (586 atoms/u.c.),[8] c_2-$Al_{39}Fe_2Pd_{21}$ (248 atoms/u.c.),[9] and the heavy-fermion compound $YbCu_{4.5}$, comprising as many as 7448 atoms in the supercell.[10] These giant unit cells contrast with elementary metals and simple intermetallics whose unit cells in general comprise from single up to a few tens of atoms only. Inside the giant unit cells the atoms are arranged in clusters with polytetrahedral local atomic order of icosahedral or decagonal symmetry as typically found in quasicrystals (QCs).

The icosahedral local order, which is incompatible with translational periodicity of a crystalline lattice, is slightly distorted in periodic structures, but remains close to that of QCs. A multitude of different coordination polyhedra leads to a large number of different atomic environments, where icosahedrally coordinated environments play the prominent role. For example, there is a large group of CMA materials whose structures are based on the 55-atom Mackay icosahedron, another group is based on the 105-atom icosahedral Bergman cluster.[2] Consequently, in CMAs there exist two substantially different physical length scales—one defined by the cluster substructure and the other by the unit-cell parameters—so that interesting physical properties may appear from the competition between these different length scales.

A particular property of CMA structures is the possibility of additional disorder in the giant unit cells apart from that due to atomic substitution, interstitials or creation of vacancies, which are also present in simple intermetallics. In CMAs there exist also (i) *split* occupation, where two sites are alternatively occupied because they are too close in space to be occupied simultaneously and (ii) *configurational* disorder resulting from statistically varying orientations of a particular subcluster inside a given cage of the atoms.

The structures of the giant-unit-cell CMA compounds can be described with reference to a six-dimensional hypercubic lattice in the framework of the cut-and-projection formalism originally developed to describe QCs.[11] The only difference is that a suitable rational cut is employed rather than the irrational one used for the QC lattice. For that reason the giant-unit-cell intermetallics are frequently referred to in the literature as rational approximants to QCs.

Although determining the structure of giant-unit-cell intermetallics has attracted the attention of crystallographers for a very long time (the pioneering work[3] on $NaCd_2$ dates back to 1923), studies of their physical properties remain scarce. The intense research on QCs in the past two decades—mostly ternary and quaternary intermetallic phases—has also brought about dramatic technical advances in single-crystal growth procedures for other intermetallic compounds.[12] Procedures were developed for the treatment of complex alloys containing incongruent phases and "inconvenient" elements, possessing, e.g., high vapor pressure. Consequently, fairly high-quality single-crystalline samples of several CMAs are now available. The clustering feature of CMA structures together with the above-mentioned competing physical length scales may have a significant impact on the physical properties of the material, such as the electronic structure and the lattice dynamics. On this basis, giant-unit-cell materials can exhibit transport properties, like a combination of metallic electrical conductivity with low thermal conductivity, and electrical and thermal resistances that are tunable by varying the composition. The cluster structure is also at the origin of an enhanced hydrogen-storage capacity,[13] thus pointing to a potential for energy-storage applications.

Among the CMA materials, an interesting family of related structures was revealed in the Al-Pd alloys system[14,15] and its ternaries with transition metals (Mn, Fe, Co, Rh).[16–20] CMA phases were observed in specific compositional ranges and, depending on composition, exhibit a row of orthorhombic structures and those aperiodic in one dimension.[20] The simplest regular structure discovered first in the Al-Pd-Mn (Refs. 16 and 17) system, designated as ξ', contains 320 atoms in its unit cell. Some physical properties of single-crystalline samples of this compound grown by the self-flux technique were already reported.[21] Recently we succeeded to grow centimeter-size single crystals of the ξ' phase and the related Ψ phase (containing about 1500 atoms in the unit cell) with the composition $Al_{74}Pd_{22}Mn_4$ using the Bridgman technique.[12] Here we present a study of their magnetic, electrical, and thermal transport and thermoelectric properties. As we shall demonstrate, the studied material exhibits some peculiar features, like a temperature-compensated electrical resistivity between 300 and 4 K. These findings are compared to the properties of the Al-Pd-Mn icosahedral phase stable at the neighboring compositions, typically about $Al_{70}Pd_{22}Mn_8$.

II. STRUCTURAL CONSIDERATIONS

Traditionally, the Al-Pd-Mn ξ' structure is described in terms of an orthorhombic unit cell (space group *Pnma*) with the lattice parameters[16,17] $a=2.354$ nm, $b=1.656$ nm, and $c=1.234$ nm. More recent transmission electron microscopy (TEM) investigations revealed other structures closely related to this and frequently forming in the same Al-Pd-Mn samples,[17,12] resulting in structural inhomogeneity of the samples. Those and other structures were described in detail in Al-Pd,[14,15] Al-Pd-Co,[19] and Al-Pd-Fe (Refs. 18 and 20) alloy systems. In several earlier investigations the fact of structural inhomogeneity was not considered and the label ξ' was generalized to represent a family of structures comprising the ξ' phase and a set of related structures. A brief description of these phases, based on previous work,[12,20] is given below. Due to historical reasons, different nomenclatures are used for the same structures observed in different alloy systems. In Al-Pd-Fe,[20] four stable orthorhombic structures labeled ε_6 (corresponding to ξ'), ε_{16}, ε_{22}, and ε_{28} (corresponding to Ψ) are described. According to this nomenclature, the index of ε is the number l of the strong $(00l)$ diffraction reflection corresponding to the interplanar spacing of about 0.2 nm. The lattice parameters $a\approx 2.35$ nm and $b\approx 1.66$ nm are common to all ε phases and only slightly depend on composition, while the c parameters are ≈ 1.23, 3.24, 4.49, and 5.70 nm, i.e., approximately of the ratio $1:(1+\tau):(2+\tau):(3+\tau)$, where τ is the golden mean. Apart from these periodic structures, also structures with the same a and b parameters, but aperiodic in the c direction are revealed at intermediate compositions. These aperiodic phases are also concluded to be stable and their formation due to specific substitution mechanism allows the structural continuity inside the wide compositional region. Qualitatively similar picture was observed in all studied alloy systems of Al with Pd and a third transition metal. In the following we will refer to these structures as to the variants of the ε family and use the labels ξ' for the $c\approx 1.23$ nm phase (320 atoms in the unit cell) and Ψ for the $c\approx 5.70$ nm phase (about 1500 atoms in the unit cell). These two phases also correspond to the sample materials studied in this work.

The structures of the ε phases consist of atomic clusters of the distorted Mackay-type icosahedra. In ξ' $(=\varepsilon_6)$, the cluster centers are located at the vertices of flattened hexagons[16,22] [Figs. 1(a) and 1(b)]. The planes of alternatively arranged flattened hexagons are oriented perpendicular to the [0 1 0] direction.[16] These planes form a stacked-layer structure with three different flat and one puckered layer, each of them exhibiting local pentagonal or decagonal symmetry. The structure variants with larger c parameter are based on a characteristic type of line defect[17] called a "phason line" [Fig. 1(c)], having an extension along the [0 1 0] direction. The defect consists of local rearrangements or "flips" of clusters, where several flattened hexagons merge into a banana-shaped polygon and an attached pentagon. These flips can be regular or irregular. The defects are mobile along the [0 0 1] direction. If a high density of phason lines is present in the structure, they tend to arrange closely neighbored along the [1 0 0] direction, forming so-called phason planes.[23,24] The variants of the ε family can be understood in terms of periodic arrangement of these phason planes. If a high density of phason planes is present in the structure, they tend to stack periodically along the [0 0 1] direction. Different densities of

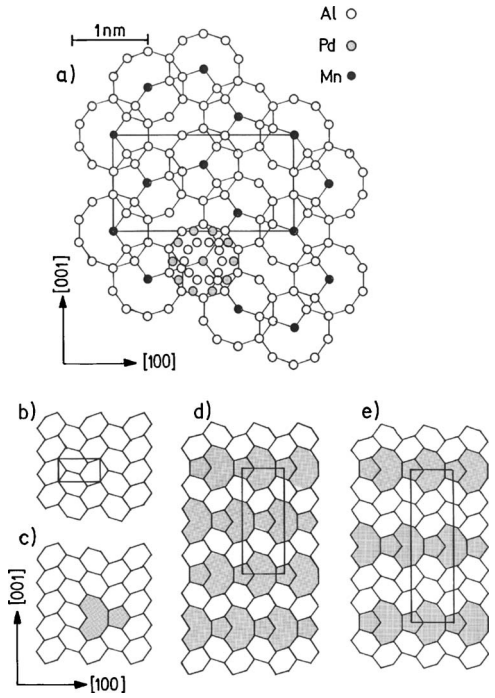

FIG. 1. **(a)** Schematic representation of the ξ' Al-Pd-Mn structure [the so-called I-layer (Ref. 22) is shown] with tenfold units indicating Mackay icosahedra. The complete structure of one of the icosahedra (projected on the plane) is shown below the rectangle that marks the projected unit cell. The flattened hexagonal tiles are obtained by connecting the centers of Mackay icosahedra. **(b)** Scheme of the ideal ξ' structure ($c=1.23$ nm), **(c)** a phason-line defect, **(d)** the Ψ structure ($c=5.7$ nm), and **(e)** a structure (Ref. 12) with $c=8.17$ nm. The respective unit cells are shown also.

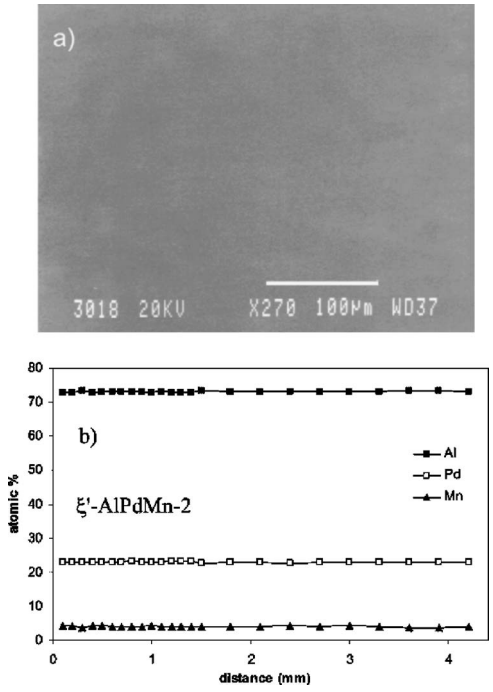

FIG. 2. **(a)** BSE image of the -AlPdMn-1 sample, demonstrating single-phase material with no inclusion of secondary phases. **(b)** Compositional heterogeneity test of the -AlPdMn-2 sample by performing a line-profile analysis of the concentration of each constituent element along the long dimension of the sample.

phason planes lead to different stacking distances [Figs. 1(d) and 1(e)] and, hence, to different c-lattice parameters.

III. SAMPLE PREPARATION

The sample material was grown by the Bridgman technique, for details see Ref. 12. Three samples were investigated under nominally the same experimental conditions. The samples were selected on the basis of previous TEM examinations. Two samples were cut from the same ingot and consisted of the major ξ' phase (referred to as the samples ξ'-AlPdMn-1 and ξ'-AlPdMn-2), whereas the third sample, of the major Ψ phase (referred to as Ψ-AlPdMn), was from another batch. The samples were shaped in the form of rectangular prisms with the long axis along the [0 1 0] direction. Their dimensions were $1.8\times1.6\times5$ mm^3 (ξ'-AlPdMn-1), $1.8\times1.6\times4.2$ mm^3 (ξ'-AlPdMn-2), and $1\times1.2\times2.6$ mm^3 (Ψ-AlPdMn). In order to determine the chemical composition of the samples and to check for the presence of secondary phases, scanning electron microscope (SEM) investigations were made with a JEOL JSM 5800 microscope. The samples were polished using conventional metallographic techniques, with the final stage involving the use of a 1/4 μm diamond paste to produce a scratch-free surface finish. For all three samples the backscattered electron (BSE) images showed featureless, homogeneous gray patterns [Fig. 2(a)], confirming that the samples are single-phase crystals with no inclusion of secondary phases. The chemical composition of the samples was determined using energy-dispersive x-ray spectroscopy (EDXS) with a focused beam. Each sample was measured at three random points on the surface. The average compositions of the samples were determined to be $Al_{73}Pd_{22.9}Mn_{4.1}$ for the ξ'-AlPdMn-1, $Al_{72.7}Pd_{23.2}Mn_{4.1}$ for the ξ'-AlPdMn-2, and $Al_{72.9}Pd_{22.9}Mn_{4.2}$ for the Ψ-AlPdMn with the uncertainty for the concentration of each element ±0.5. In order to check for the possible compositional heterogeneity, we performed a line-profile analysis along the long dimension of the samples. A compositional profile of the ξ'-AlPdMn-2 sample, to be considered as representative of all three samples, is displayed in Fig. 2(b). No variation of the concentrations of any of the three constituent elements (Al, Pd, and Mn) was observed over the total length of the crystal, confirming its high compositional homogeneity. The SEM results thus show that the samples are single-phase homogeneous materials, free of grain boundaries and secondary phases.

IV. MAGNETIC MEASUREMENTS

The magnetization as a function of the magnetic field, $M(H)$, and the temperature-dependent magnetic susceptibility, $\chi(T)$, were measured with a Quantum Design superconducting quantum interference device (SQUID) magnetometer, equipped with a 5 T magnet. The susceptibility χ was investigated in the temperature interval between 300 and 2 K in a magnetic field $H=5$ kOe applied along [010] direction

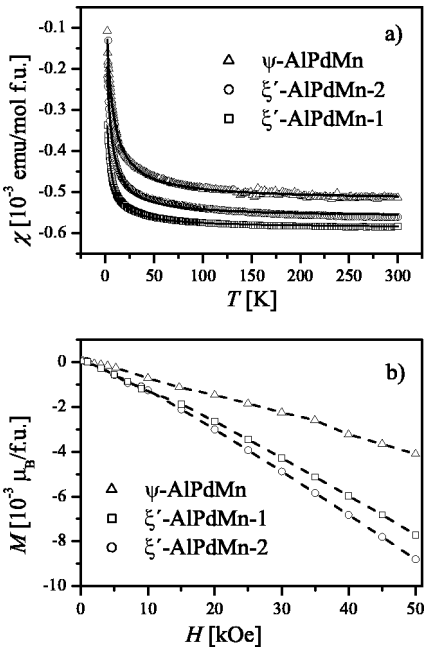

FIG. 3. **(a)** Temperature-dependent magnetic susceptibility χ in a field $H=5$ kOe (solid lines are fits described in the text) and **(b)** magnetization M as a function of the magnetic field H at $T=5$ K (the slight nonlinearity in the vicinity of $H=0$ is due to a thin ferromagnetic surface oxide layer). The dashed lines are a guide for the eye and f.u. denotes "formula unit."

[Fig. 3(a)]. In this field the $M(H)$ dependence is linear [Fig. 3(b)], so we analyze $\chi=M/H$ in the following. The $\chi(T)$ values of all three samples are negative for the whole of the investigated temperature interval, indicating a dominant diamagnetic contribution. In addition, small paramagnetic Curie-like growth of the magnetization upon cooling is observed. The $\chi(T)$ data were analyzed by the sum of a Curie term and a temperature-independent term χ_0

$$\chi = \frac{C}{T-\theta} + \chi_0, \tag{1}$$

and the fits are shown as solid lines in Fig. 3(a). The values of the parameters C (the Curie constant), θ (the Curie–Weiss temperature), and χ_0 are summarized in Table I. For an electrically conducting material one generally expects two contributions of comparable size to the temperature-independent term χ_0: the negative diamagnetic contribution due to core electrons and the positive Pauli paramagnetic contribution due to conduction electrons, $\chi_0=\chi_{dia}+\chi_{Pauli}$. The diamagnetic contribution χ_{dia} can be estimated from Pascal tables.[25] For different choices of the ionization states of the elements (e.g., $Mn^{2+}, Mn^{3+}, Mn^{4+}, Pd^{3+}, Pd^{4+}, \ldots$) the calculated χ_{dia} values are all in the range between -0.6×10^{-3} and -0.8×10^{-3} emu/mol, whereas the experimental χ_0 values are in the interval between -0.5×10^{-3} and -0.6×10^{-3} emu/mol. We, therefore, have $\chi_0\approx\chi_{dia}$, so that the diamagnetic contribution dominates over the conduction electron contribution χ_{Pauli}. This fact reflects the relatively low electrical conductivity of the studied samples (to be discussed in the next paragraph), as compared to regular metals. The dominant diamagnetic contribution to the magnetization is also observed in the $M(H)$ curves [Fig. 3(b)] obtained at 5 K, which exhibit a typical diamagnetic linear decrease with increasing H.

TABLE I. Parameters C, θ, and χ_0 obtained from the fits of the temperature-dependent magnetic susceptibility. The magnetic fraction f of Mn atoms was calculated from the Curie constants C (see text), assuming the atoms are in the Mn^{2+} state ($p_{eff}=5.9$).

Sample	C (emu K/mol)	θ (K)	χ_0 ($\times10^{-3}$ emu/mol)	f
ξ'-AlPdMn-1	1.24×10^{-3}	−3.0	−0.59	0.7×10^{-4}
ξ'-AlPdMn-2	1.92×10^{-3}	−3.2	−0.56	1.0×10^{-4}
Ψ-AlPdMn	2.89×10^{-3}	−5.4	−0.52	1.6×10^{-4}

The Curie-type dependence of the paramagnetic part of the magnetization indicates the presence of localized magnetic moments in the structure. In analogy to *i*-Al-Pd-Mn QCs, it is straightforward to attribute this magnetization to the Mn species. The small paramagnetic susceptibility, which even at 2 K is smaller than the diamagnetic core susceptibility, indicates that only a tiny fraction of the Mn atoms are magnetic. The fraction of magnetic atoms in the samples can be estimated from the values of the Curie constant C. We assume that the magnetic manganese atoms are in the Mn^{2+} state with the effective Bohr magneton number $p_{eff}=5.9$ and recalculate C from Table I (given there in units of *per mol of sample*) in units of *per mol of Mn*. From the obtained values we calculate the mean effective Bohr magneton number (the mean p_{eff} of all the Mn atoms in the sample) by using the formula[26] $\bar{p}_{eff}=2.83\sqrt{C}$. The magnetic fraction f is then obtained from $f=(\bar{p}_{eff}/p_{eff})^2$. The estimated f values of the three investigated samples are given in Table I. They are very small and of comparable magnitude, all close to 1×10^{-4}.

The small, negative values of the Curie–Weiss temperature θ (Table I) should be considered as additional fit parameters only, which slightly improve the fits in Fig. 3(a). No other experimental results suggest any antiferromagnetic interaction between the magnetic moments.

Comparing the magnetic properties of the three investigated samples, no qualitative differences were found. All the samples can be considered as diamagnets with a tiny paramagnetic Curie magnetization. The small differences between the ξ'-AlPdMn-1 and ξ'-AlPdMn-2 samples that were cut from the same ingot either reflect their tiny compositional/structural differences or are due to a variation of the experimental conditions (sample size, shape effects, etc.). The difference between the Ψ-AlPdMn sample and the other two is slightly larger, but is again small enough that it could be due to a variation of the experimental conditions. Regarding the comparison of the ξ' and Ψ magnetic properties to those of the *i*-Al-Pd-Mn QCs, the icosahedral QCs are generally substantially more magnetic, with the magnetic Mn fractions typically one to two orders of magnitude larger,[27–29] $f\approx10^{-3}$–10^{-2}. This is despite only about two times higher Mn concentration in the QC state. The magnetic fraction of the icosahedral phase was found to be strongly dependent on the thermal history (i.e., it has decreased after thermal an-

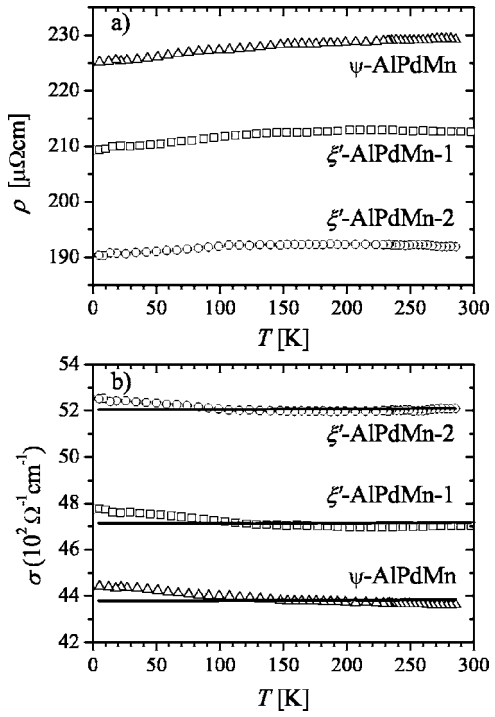

FIG. 4. **(a)** Temperature-dependent electrical resistivities ρ and **(b)** the conductivities ($\sigma=\rho^{-1}$) fitted with the spectral conductivity model (solid lines).

nealing), which was attributed to the concentration of vacancies[29] in the lattice. Similar to the ξ' phase, also some other QC approximants in the Al-Pd-Mn alloy system (the cubic 2/1-$Al_{70}Pd_{24}Mn_{65}$, the orthorhombic Taylor phase T-$Al_{78.5}Pd_{4.9}Mn_{16.6}$) were found nonmagnetic, whereas paramagnetic behavior was detected in the Mn-rich T-$Al_{73.1}Pd_{5.2}Mn_{21.7}$ and 1/1-$Al_{68}Pd_{11}Mn_{14}Si_7$ phases.[30] Finally, we stress that our analysis was made using the assumption that the total observed Curie magnetization of the investigated samples originates from the Mn atoms and is thus intrinsic to the ξ' and Ψ phases. In view of the smallness of the paramagnetic magnetization, indicating that only about 100 ppm of all the Mn atoms are magnetic, and of the ever-present extrinsic magnetic impurities at the level of about 10 ppm due to the finite purity of the starting elements used for the crystal growth, the magnetization very likely contains both the Mn and the impurity moments. Therefore, the f values from Table I should be considered as an upper limit for the magnetic Mn fractions in the investigated samples. Similar small magnetic fraction (1 Mn out of every 60 000) and the conclusion on the significant contribution of impurity moments to the Curie magnetization was obtained also for the $Al_{72}Pd_{25}Mn_3$ composition.[21]

V. ELECTRICAL RESISTIVITY

The electrical resistivity $\rho(T)$ was determined in the temperature interval between 300 and 4 K using the standard four-terminal technique. The resistivity was measured along [0 1 0] direction of the samples and the data are displayed in Fig. 4(a). The room-temperature values are $\rho_{300\ K}=213\ \mu\Omega$ cm for the ξ'-AlPdMn-1 sample, $\rho_{300\ K}=192\ \mu\Omega$ cm for the ξ'-AlPdMn-2 and $\rho_{300\ K}=229\ \mu\Omega$ cm for the Ψ-AlPdMn. The remarkable feature is the very small temperature variation of the resistivity in all three samples: $R=(\rho_{300K}-\rho_{4K})/\rho_{300K}=1.4\%$ for the ξ'-AlPdMn-1, $R=0.5\%$ for the ξ'-AlPdMn-2, and $R=1.7\%$ for the Ψ-AlPdMn. Such a nearly temperature-compensated resistivity represents an intermediate case between the positive-temperature-coefficient (PTC) resistivity of metals (originating from the scattering of electrons by phonons) and the negative-temperature-coefficient (NTC) resistivity commonly found in metallic glasses and QCs (due to a gradual electron localization caused by disorder/quasiperiodicity upon cooling). For the CMA materials, the temperature-compensated $\rho(T)$ offers the following qualitative explanation based on competition between the two above-mentioned physical length scales. The large-scale periodicity promotes the regular metallic PTC resistivity, whereas the polytetrahedral local order favors the NTC resistivity, and the competition of both results in a nearly temperature-independent $\rho(T)$. A similar situation of a nearly temperature-compensated $\rho(T)$ was also found recently in the large-unit-cell QC approximants of the Al-Cr-Fe family.[31]

The differences in the absolute resistivity values of the three samples are small, being scattered at, e.g., room temperature in the interval ±8% around the average value $\bar{\rho}_{300K}=211\ \mu\Omega$ cm. While the measurement error in the temperature dependence of ρ of each sample is small, of the order 1%, there are larger errors present relating to the sample-geometry determination and to the homogeneity of the current through the samples that affect the absolute value of the resistivity. Due to these effects, the absolute resistivity values shown in Fig. 4(a) may be in error by up to 20%, which is larger than the scattered range of the experimental ρ values. From this point of view, the absolute resistivity values of all three samples are within the estimated error range, showing no significant differences.

Relating the resistivities of the investigated ξ' and Ψ phases to those of the i-Al-Pd-Mn QCs, the ρ values of icosahedral samples are one order of magnitude larger (ranging typically from 1000 up to 4000 $\mu\Omega$ cm). The $\rho(T)$ of the i-Al-Pd-Mn QCs is, however, drastically different. The resistivities of QCs often exhibit negative temperature coefficients, but the magnitude of the NTC varies considerably between samples. In addition, the $\rho(T)$ of i-Al-Pd-Mn QCs in many cases displays a maximum[32–36] between room temperature and 4 K and sometimes also a minimum[33–35] at still lower temperatures. Whereas the maximum in $\rho(T)$ can be explained either by weak localization of the conduction electrons[37] or by a magnetic effect,[38] the low-temperature minimum was attributed to the Kondo effect.[33]

In order to gain a microscopic, theoretical insight into the origin of the temperature-compensated resistivity of the ξ' and Ψ samples, we attempted to perform an *ab initio* calculation of the electronic density of states (DOS) by the linear muffin-tin orbital (LMTO) method on the structural cluster model by Boudard *et al.*[16] The main difficulty we encountered was the many atomic positions in the unit cell with fractional occupancies. Several test models with particular

choices of occupied and unoccupied sites did not yield converging results, so that this kind of theoretical approach turned out to be ineffective. For that reason we instead used the simplified spectral-conductivity model,[39–41] which assumes the existence of a pseudogap in the DOS at the Fermi energy E_F of a particular shape—a paraboliclike wide pseudogap with a superimposed narrow pseudogap. The increasingly deeper narrow-pseudogap component leads to an increase in the resistivity, so that the model was successfully used in the past to explain the progressive transition of ρ from low-resistivity amorphous metals to approximants and highly resistive QCs.[39,42] For approximants of relatively low resistivity ($\rho \approx 100 \mu\Omega$ cm) one expects that the narrow pseudogap component will disappear and only the (Hume–Rothery-like) wide pseudogap will be present. This is supported by theoretical DOS calculations, where a broad shallow minimum at the E_F was found in several CMA systems—the Bergman phase[43,44] $Mg_{32}Al_{13}Zn_{36}$, the cubic R-phase[45] Al_5CuLi_3, and the Mackay-type approximant[46] $Mg_{57}Pd_{13}$.

The temperature-dependent electrical conductivity $\sigma(T)$ (the inverse resistivity, $\sigma=\rho^{-1}$) is obtained from the Kubo–Greenwood formula[47,48]

$$\sigma(T) = \int dE\ \hat{\sigma}(E) \left[-\frac{\partial f(E,\mu,T)}{\partial E} \right], \tag{2}$$

where $\mu \approx E_F$ is the chemical potential, $f(E,\mu,T)$ is the Fermi–Dirac distribution function, and $\hat{\sigma}(E)$ is the spectral conductivity, which is the only material-dependent quantity in Eq. (2). In the vicinity of the E_F the spectral conductivity can be approximated by a paraboliclike wide pseudogap[39]

$$\hat{\sigma}(E) = A_0 + A_1(E-\mu) + A_2(E-\mu)^2, \tag{3}$$

where the A_1 term accounts for the possible asymmetry. This Ansatz yields a temperature-dependent conductivity of the form

$$\sigma(T) = \sigma_0 + \sigma_1 T^2, \tag{4}$$

with $\sigma_0=A_0$ and $\sigma_1=(\pi^2/3)k_B^2 A_2$. Here it is worth noting that from the measured $\sigma(T)$ we can obtain only the parameters A_0 and A_2 (through σ_0 and σ_1), whereas complementary measurements of the thermoelectric power (to be discussed later) can provide information about the parameter A_1. A truly temperature-independent conductivity (or resistivity) is obtained in the case $\sigma_1 \propto A_2 = 0$. In real cases, it is enough that $\hat{\sigma}(E) \approx A_0 = \sigma_0$ for energies $(E-\mu) \leqslant k_B T$. This means that the DOS within the pseudogap should not change noticeably over the energy scale covered by the derivative $(-\partial f/\partial E)$ of the Fermi–Dirac function (that is centered at the Fermi energy and has a full width at half height of about $3.5k_BT$). Thus, the existence of a broad shallow minimum in the pseudogap, not changing noticeably over about $3.5k_BT$ around the Fermi level (where, e.g., $3.5k_BT=90$ meV at $T=300$ K), is at the origin of the temperature-independent resistivity within the spectral-conductivity model.

The theoretical fits with Eq. (4) to the conductivity data [the inverse data of Fig. 4(a)] are displayed in Fig. 4(b). Here it is important to stress that Eq. (4) cannot reproduce the tiny residual temperature dependence of $\sigma(T)$ observed below 100 K for all three samples. For that reason the fits (solid lines) were restricted to data points above 100 K, demonstrating the limited applicability of the spectral conductivity model employed here to describe the resistivity of the ξ' and Ψ material. The parameter A_2 was restricted to positive values (a condition for the existence of a pseudogap) and the fit parameter values σ_0 and σ_1 are listed in Table II. These values show that $\sigma_0 \gg \sigma_1 T^2$ for all temperatures of interest, which indicates an almost energy-independent spectral conductivity (at least for $(E-\mu) \leqslant (k_BT)$, and consequently, an almost temperature-independent conductivity.

TABLE II. Electrical conductivity parameters of the ξ' and Ψ Al-Pd-Mn samples, obtained from the theoretical fits in Fig. 4(b) using Eq. (4).

Sample	σ_0 (Ω^{-1} cm^{-1})	σ_1 (10^{-5} Ω^{-1} cm^{-1} K^{-2})
ξ'-AlPdMn-1	4712	6.2
ξ'-AlPdMn-2	5206	4.6
Ψ-AlPdMn	4380	6.3

VI. THERMAL CONDUCTIVITY

The thermal conductivities were measured between 8 and 300 K along [010] direction using an absolute steady-state heat-flow method. The thermal flux through the samples was generated by a 1 kΩ RuO_2 chip resistor, glued to one end of the sample, while the other end was attached to a copper heat sink. The temperature gradient across the sample was monitored by a chromel-constantan differential thermocouple. The temperature dependence of the thermal conductivity parameter $\kappa(T)$ of all three samples is displayed in Fig. 5. The $\kappa(T)$ values at 280 K are 8.6 W/mK for the ξ'-AlPdMn-1 sample, 7.3 W/mK for the ξ'-AlPdMn-2 and 5.0 W/mK for the Ψ-AlPdMn. These low $\kappa(T)$ values are of the same order as those of *i*-Al-Pd-Mn QCs,[49,50] where they are considered to be a consequence of both the low electronic DOS at the E_F and the nonperiodicity of the lattice, making the electronic and lattice contributions to the heat transport small. The elec-

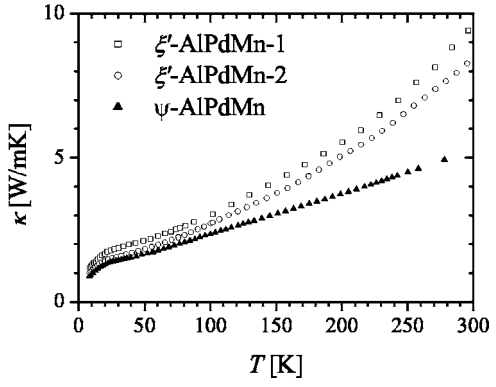

FIG. 5. Temperature-dependent thermal conductivities $\kappa(T)$ between 8 and 300 K.

tronic contribution to the thermal conductivity κ_{el} can be calculated using the Wiedemann–Franz law and the measured electrical resistivity $\rho(T)$ data, presented in Fig. 4(a). The calculation of the Lorenz number for the *i*-Al-Cu-Fe QCs has shown[39] that its "relaxation-time-approximation" value $L_0=2.44\times10^{-8}$ W Ω K^{-2} may have a correction of the order of 10%. For that reason we assumed a slight modification of the Wiedemann–Franz law

$$\kappa_{el}=(1+\varepsilon)L_0T/\rho, \tag{5}$$

where the correction factor ε (of the order 0.1) should be determined from the fit. ε may also be considered as a compensating factor for the errors in the sample-geometry estimation in both the resistivity and the thermal conductivity experiments.

The lattice contribution to the thermal conductivity $\kappa_l=\kappa-\kappa_{el}$ is analyzed, in analogy to QCs and amorphous solids, by considering the propagation of long-wavelength phonons within the ξ' and Ψ structures and, at elevated temperatures, the hopping of localized vibrations. While the long-wavelength phonons may be analyzed within the Debye model, the hopping of localized vibrations represents thermally activated motion, which we assume can be described by an activation energy E_a. Within this model, hopping yields a contribution to the thermal conductivity

$$\kappa_H=\kappa_H^0\exp(-E_a/k_BT), \tag{6}$$

where κ_H^0 is a constant. The Debye thermal conductivity is written as[51]

$$\kappa_D=C_DT^3\int_0^{\theta_D/T}\tau(x)\frac{x^4e^x}{(e^x-1)^2}dx. \tag{7}$$

Here $C_D=k_B^4/2\pi^2\bar{\nu}\hbar^3$, $\bar{\nu}$ is the average sound velocity (defined by $3/\bar{\nu}^3=1/\nu_L^3+2/\nu_T^3$, where ν_L and ν_T are the longitudinal and transversal sound velocities, respectively), θ_D is the Debye temperature, τ is the phonon relaxation time, and $x=\hbar\omega/k_BT$, where $\hbar\omega$ is the phonon energy. The different phonon-scattering processes are incorporated in the relaxation time $\tau(x)$ and we assume that Matthiessen's rule is valid, $\tau^{-1}=\Sigma\tau_j^{-1}$, where τ_j^{-1} is a scattering rate related to the *j*th scattering channel. In amorphous solids and QCs the two dominant phonon-scattering processes at low temperatures are Casimir scattering at the sample boundaries and scattering on the tunneling states. Because in our experiments, which were performed between 300 and 8 K, we do not really enter the low-temperature regime, these two processes may be neglected. There are, however, two other processes that dominate thermal conduction in the investigated temperature regime. First, are structural defects of stacking-fault type, for which the scattering rate is given by[52]

$$\tau_{sf}^{-1}=\frac{7}{10}\frac{a^2}{\bar{\nu}}\gamma^2\omega^2N_s. \tag{8}$$

Here a is a lattice parameter, γ is the Grüneisen parameter, and N_s is the linear density of stacking faults. For the convenience of the fitting procedure, we rewrite $\tau_{sf}^{-1}=Ax^2T^2$ (note that, since $x^2\propto T^{-2}$, τ_{sf}^{-1} does not show an explicit temperature dependence). The second scattering mechanism is the *umklapp* processes. In crystals, *umklapp* scattering rate is described by an exponential factor, $\tau_{um}^{-1}\propto\omega^2T\exp(-\theta_D/\beta T)$, where β is dimensionless parameter of the order one. In QCs and approximants, *umklapp* scattering can be described by a power-law-type frequency dependence and temperature dependence of the scattering rate[53] $\tau_{um}^{-1}\propto\omega^2T^4$. Many different power-law expressions, such as $\tau_{um}^{-1}\propto\omega^3T,\omega^2T^2,\omega^2T^4$, can be found in the literature, so that we assume phenomenologically $\tau_{um}^{-1}=Bx^\alpha T^4$, where the exponent α (yielding a power-law dependence $\tau_{um}^{-1}\propto\omega^\alpha T^{4-\alpha}$) should be determined from the fit.

The thermal conductivity data of Fig. 5 were fitted, using Eqs. (5)–(7), by the expression

$$\kappa(T)=\kappa_{el}(T)+\kappa_D(T)+\kappa_H(T), \tag{9}$$

where $\tau^{-1}=\tau_{sf}^{-1}+\tau_{um}^{-1}$. Based on the specific-heat data,[54] the Debye temperatures of the related *i*-Al-Pd-Mn QCs were commonly found to be close to 500 K. We assumed that the situation is similar in the ξ' and Ψ samples and made the fit with a fixed $\theta_D=500$ *K* value. Since our $\kappa(T)$ data are available only up to 300 K, it turned out that the fit was insensitive to a slight change of this θ_D value. The Debye constant C_D was also not taken as a free parameter, but was instead calculated by using $\bar{\nu}=4004$ ms^{-1}, a value determined for the *i*-Al-Pd-Mn from ultrasonic data.[55] There still remain a number of fit parameters involved in the fitting procedure—ε for the electronic contribution, κ_H^0 and E_a for the hopping contribution and A, B, and α for the Debye contribution. In spite of the excellent fits of the $\kappa(T)$ data obtained with Eq. (9), to be presented in the following, and of the reasonable values of the fit parameters, the fits should not be considered more than just qualitative.

The theoretical fits of $\kappa(T)$ for the ξ'-AlPdMn-1 [Fig. 6(a)], ξ'-AlPdMn-2 [Fig. 6(b)], and Ψ-AlPdMn [Fig. 6(c)] samples using Eq. (9) show good agreement with the experimental data over the whole investigated temperature range, and the fit parameters are given in Table III. On all graphs, the individual contributions $\kappa_{el}(T)$, $\kappa_D(T)$ and $\kappa_H(T)$ to the total $\kappa(T)$ are also displayed. Due to the very small temperature dependence of $\rho(T)$ that enters the Wiedemann–Franz law, the electronic contribution $\kappa_{el}(T)$ exhibits practically linear temperature dependence and the correction factor ε was found to be either small (amounting to 0.16 for the ξ'-AlPdMn-1 and ξ'-AlPdMn-2 samples) or negligible (3×10^{-2} for the Ψ-AlPdMn). The Debye contribution $\kappa_D(T)$ exhibits a maximum at about 40 K and a decrease at higher temperatures. Similar behavior is commonly found in periodic solids, where it is attributed to *umklapp* processes and phonon-phonon scattering.[56] For all three samples, the hopping contribution κ_H becomes significant above 100 K. The activation energies for hopping were found to be similar for the ξ'-AlPdMn-1 and ξ'-AlPdMn-2 samples ($E_a\approx55$ meV), whereas the $E_a\approx21$ meV of the Ψ-AlPdMn is about two times smaller. This smaller E_a value reflects the considerably less steep $\kappa(T)$ increase at temperatures above 100 K of the Ψ-AlPdMn sample, as compared to the other two (see Fig. 5). The above E_a values correlate with the inelastic neutron (INS) (Refs. 57–59) and x-ray[60] scattering experiments on

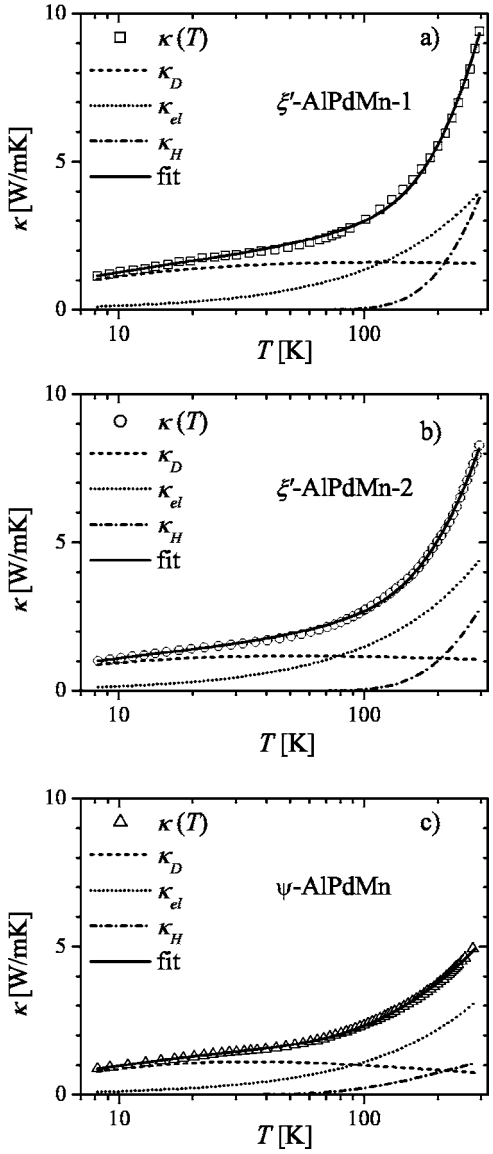

FIG. 6. **(a)** Temperature-dependent thermal conductivity $\kappa(T)$ (on the ln T scale) of the ξ'-AlPdMn-1 sample reproduced theoretically (solid line) by Eq. (9). The three contributions to the total $\kappa(T)$ are shown separately: the electronic contribution κ_{el}—dotted line, the Debye contribution κ_D—dashed line, and the hopping contribution κ_H—dash-dot line. In **(b)**, the same analysis is shown for the ξ'-AlPdMn-2 sample and in **(c)** for the Ψ-AlPdMn.

i-Al-Pd-Mn QCs, where dispersionless vibrational states were identified for energies higher than 12 meV. In QCs such dispersionless states indicate localized vibrations and are considered to be a consequence of a dense distribution of energy gaps in the phonon excitation spectrum. This prevents extended phonons from propagating through the lattice, whereas localized vibrations may still be excited. Therefore, localized vibrations also appear to be present in the giant-unit-cell ξ' and Ψ Al-Pd-Mn material, where their origin may be attributed to the icosahedral cluster substructure. The parameter A, which is for all samples close to 10^7 s^{-1} K^{-2}, makes it possible to estimate the linear density of stacking faults N_s. We take typical values for the lattice parameter $a \approx 1$ nm and the Grüneisen parameter $\gamma \approx 2$ and get $N_s = 10A\bar{v}\hbar^2/7a^2\gamma^2k_B^2 = 0.8\ \mu\text{m}^{-1}$. This micrometer-scale N_s value is comparable to those reported for *i*-Al-Pd-Mn,[61] *i*-Al-Cu-Fe,[61] *i*-Zn-Mg-Y,[62] and decagonal *d*-Al-Ni-Co (Ref. 63) QCs. The stacking-faultlike structural defects may thus be considered as the source of phonon scattering at low temperatures in the ξ' and Ψ samples. The parameters B and α define phonon scattering by *umklapp* processes in a phenomenological way. The α values of the three samples are between 3.5 and 3.9, but these values are significantly affected by other fit parameters and should be considered as indicative only. As the frequency and temperature dependences of the *umklapp* term were assumed to be $\tau_{um}^{-1} \propto \omega^\alpha T^{4-\alpha}$, the above α values indicate some similarity to the modified quasiumklapp scattering rate $\tau_{um}^{*-1} \propto \omega^3 T$, used for the analysis of the thermal conductivity of *i*-Zn-Mg-Y.[62]

TABLE III. Fit parameters of the thermal conductivity $\kappa(T)$ from Fig. 6.

Parameter	ξ'-AlPdMn-1	ξ'-AlPdMn-2	Ψ-AlPdMn
ε	0.16	0.16	0.03
E_a	57 meV	53 meV	21 meV
κ_H^0	36 W/mK	22 W/mK	2.5 W/mK
A	5.9×10^6 s^{-1} K^{-2}	6.4×10^6 s^{-1} K^{-2}	9.6×10^6 s^{-1} K^{-2}
B	2.1×10^4 s^{-1} K^{-4}	3.2×10^4 s^{-1} K^{-4}	2.2×10^4 s^{-1} K^{-4}
α	3.9	3.8	3.5

It is interesting to compare the ratio of the electronic and lattice contributions to the thermal conductivity of the ξ' and Ψ samples. At 280 K we find, for the ξ'-AlPdMn-1, $\kappa_{el} = 3.3$ W/mK and $\kappa_l = \kappa - \kappa_{el} = 5.3$ W/mK with the ratio $\kappa_{el}/\kappa_l = 0.62$. For the ξ'-AlPdMn-2 we get $\kappa_{el} = 3.6$ W/mK, $\kappa_l = 3.7$ W/mK, and $\kappa_{el}/\kappa_l = 0.97$, whereas for the Ψ-AlPdMn we get $\kappa_{el} = 2.0$ W/mK, $\kappa_l = 3.0$ W/mK, and the ratio $\kappa_{el}/\kappa_l = 0.67$. For all samples, κ_{el} and κ_l are thus of comparable size at room temperature. This is different from both simple metals, where the electronic contribution is usually 1–2 orders of magnitude larger than the lattice contribution, and Al-based QCs, where electrons carry less than 1% of the heat. From this point of view, the investigated ξ' and Ψ giant-unit-cell materials lie somewhere between metals and QCs.

VII. THERMOELECTRIC POWER

The thermopower measurements were performed at between 300 and 4 K by applying a differential method with two identical thermocouples (chromel-gold with 0.07% iron), attached to the sample with silver paint. The thermoelectric power data [the Seebeck coefficient $S(T)$] are shown in Fig. 7. The thermopowers of all three investigated samples are negative across the whole investigated temperature interval, indicating that electrons are the dominant charge carriers. The room-temperature S values are rather small, ranging between −4.7 and −8 μV/K. While the ξ'-AlPdMn-1 and ξ'-AlPdMn-2 samples exhibit a relatively smooth temperature variation of $S(T)$, the thermopower of the Ψ-AlPdMn

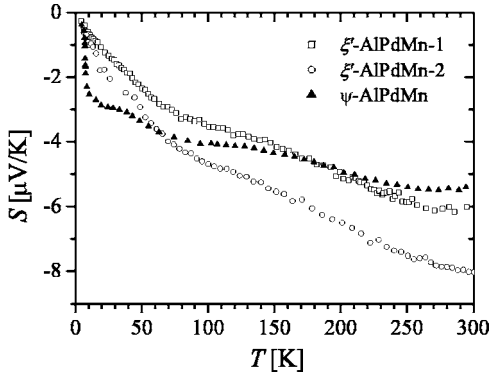

FIG. 7. Thermoelectric power $S(T)$ between 4 and 300 K.

sample shows a strong (absolute) increase between 4 and 8 K, followed by a weaker increase at higher temperatures. For all samples, $S(T)$ shows several changes of slope within the investigated temperature range. The thermopower can be, in principle, analyzed with the same spectral conductivity model as used for the analysis of the electrical conductivity. Using Eq. (3), the thermopower can be related to the parameter A_1 using the Mott formula[64] $S^{Mott}(T) = -(\pi^2/3)(k_B^2 T/|e|)\{(d\hat{\sigma}/dE)/\hat{\sigma}\}_{E=E_F} = -(\pi^2/3)(k_B^2 T/|e|)(A_1/A_0)$. This formula yields smooth $S(T)$ temperature behavior and cannot reproduce the changes of slope, observed experimentally at several temperatures in the $S(T)$ data of all three samples, so we skip the analysis of the thermopower with this model. However, considering this approximation (valid for low temperatures), we can see that $A_1 \neq 0$ in order to explain finite $S(T)$. This means that the spectral conductivity $\hat{\sigma}(E)$ of Eq. (3) has to be slightly asymmetric. Moreover, a crude estimate of the Fermi energy can be obtained for the ξ'-AlPdMn-1 sample, which exhibits the smoothest $S(T)$ behavior. Approximating its $S(T)$ by a linear function (with zero at 0 K and $S_{300\ K} \approx -6\ \mu$V/K, yielding $S/T = -0.02\ \mu\text{V/K}^2$), and using the expression $S = -(\pi^2 k_B^2/2|e|E_F)T$ that is valid in the free-electron limit with the electron collision time independent of energy,[65] we obtain $E_F = 1.8$ eV.

VIII. SUMMARY AND CONCLUSIONS

We investigated magnetic, electrical, and thermal transport and thermoelectric properties of the giant-unit-cell ξ' and Ψ CMA phases in the Al-Pd-Mn system. The materials were Bridgman-grown, concentrationally homogeneous single-crystalline samples, free of grain boundaries and of secondary phases. All measurements were performed along the [0 1 0] crystalline direction. As the investigated physical properties are expected to be spatially anisotropic, additional measurements should be performed in the future along the other two crystalline directions of the orthorhombic structure, in order to obtain complete information on the tensorial character of the physical parameters. Magnetic susceptibility measurements have shown that the samples are diamagnets with a tiny paramagnetic Curie-like magnetization, which is smaller than the diamagnetic contribution, even at the lowest investigated temperature of 2 K. The estimated fraction of magnetic Mn atoms (assumed to be in the Mn^{2+} state) in all samples is about 100 ppm, where external impurities at the level of 10 ppm contribute to the observed Curie magnetization as well. The electrical resistivity is temperature independent to within less than 2% in the investigated interval between 300 and 4 K. The ρ value of about 200 $\mu\Omega$ cm is one to two orders of magnitude larger than the resistivities of simple metals and alloys, and one order smaller than those of *i*-Al-Pd-Mn QCs. The origin of the almost temperature-compensated resistivity was analyzed in terms of the spectral conductivity model, where this feature is attributed to the existence of a wide, shallow pseudogap in the electronic DOS at the Fermi energy that does not depend noticeably on the energy over an interval $(E-\mu) \leqslant k_B T$. The thermal conductivity of the $\xi'$and Ψ samples is small, comparable in magnitude to that of *i*-Al-Pd-Mn QCs. This suggests that a low electronic DOS at the E_F and a low phonon density are at the origin of the weak heat transport. While the electronic contribution κ_{el} can be described by the Wiedemann–Franz law, the lattice contribution κ_l can be reproduced by the sum of the Debye term (long-wavelength phonons) and the term due to hopping of localized vibrations. While hopping is the dominant lattice heat-carrying channel at elevated temperatures (above 100 K), the Debye term dominates at low temperatures and exhibits an insignificant maximum in $\kappa_D(T)$ at a temperature close to 40 K. At the lowest measured temperature (8 K), the scattering of phonons on stacking-faultlike defects limits the heat transport, whereas at higher temperatures, *umklapp* processes become excited. The room-temperature values of the electronic conductivities and the lattice thermal conductivities were found to be of comparable size, which is different from both simple metals and Al-based QCs. The thermoelectric power of about $-6\ \mu$V/K at room temperature is small, compatible with a low concentration of charge carriers, and negative, indicating that electrons are the majority carriers. For all samples, $S(T)$ shows several changes of slope within the investigated temperature range.

The temperature-compensated electrical resistivity and the comparable electronic and lattice contributions to the thermal conductivity allow the transport properties of the giant-unit-cell ξ' and Ψ materials to be classified between regular metals and Al-based quasicrystals. Considering that polytetrahedral local atomic order of icosahedral symmetry promotes electron and phonon localization, whereas large-scale periodicity favors their extended character, this suggests that both the electrical resistivity and the thermal conductivity (and consequently also the thermopower) are affected by the competition between the two physical scale lengths encountered in the large-unit-cell CMA materials. Regarding the differences in the studied physical properties between the investigated ξ'-AlPdMn-1, ξ'-AlPdMn-2, and Ψ-AlPdMn samples, no differences were found that would be significantly larger than the estimated experimental errors (originating from the sample size and geometry determination and the electrical current and thermal flux inhomogeneity through the samples), except for the activation energy of localized vibrations that is a factor two smaller in the

Ψ-AlPdMn sample. Therefore, the nanometric-scale structural differences of the ξ' and Ψ phases do not seem to alter the studied physical properties of the system significantly.

Regarding the important question of the role of quasiperiodicity versus periodicity on the physical properties of a solid, our results obtained on the translationally periodic single-crystalline ξ' and Ψ Al-Pd-Mn phases that are recognized as excellent quasicrystalline approximants to the icosahedral phase, can be directly contrasted to the previously reported physical properties of the *i*-Al-Pd-Mn single-grain QCs. The major differences are observed in: (i) the electrical resistivity, where the resistivities of the ξ' and Ψ phases are one order of magnitude smaller than those of *i*-Al-Pd-Mn, and exhibit temperature-compensated behavior as opposed to the NTC resistivity of *i*-QCs (indicating that the weak localization effect in the ξ' and Ψ is less strong than in *i*-QCs); (ii) the $\xi'$and Ψ phases are considerably less magnetic, the fraction of magnetic atoms being a factor 10–100 smaller than in *i*-Al-Pd-Mn QCs; (iii) the ξ' and Ψ electronic and lattice thermal conductivities at room temperature are of comparable size, whereas in *i*-QCs the electrons carry 1% of the total heat only; and (iv) the thermopower of ξ' and Ψ is negative (resembling regular metals and alloys), indicating that electrons are majority charge carriers, whereas the thermopower of *i*-Al-Pd-Mn is more complicated, sometimes observed even to change sign with a change in temperature. As the local polytetrahedral atomic order is very similar in the ξ', Ψ, and *i*-QC phases of Al-Pd-Mn, and the structural quality of the investigated samples is comparable, these differences may be considered to originate from the different long-range orders existing in these systems—the quasiperiodic order in *i*-QCs versus the translational periodicity of giant-unit-cell CMAs.

ACKNOWLEDGMENT

This work was done within the 5th Framework EU project "Smart Quasicrystals" (Contract No. G5RD-CT-2001-00584).

[1] The term "structurally complex alloy phases" or SCAPs is also sometimes used in literature.
[2] See, for a recent review, K. Urban and M. Feuerbacher, J. Non-Cryst. Solids **334&335**, 143 (2004).
[3] L. Pauling, J. Am. Chem. Soc. **45**, 2777 (1923).
[4] L. Pauling, Am. Sci. **43**, 285 (1955).
[5] G. Bergman, J. L. T. Waugh, and L. Pauling, Acta Crystallogr. **10**, 254 (1957).
[6] S. Samson, Acta Crystallogr. **19**, 401 (1965).
[7] S. Samson, in *Developments in the Structural Chemistry of Alloy Phases*, edited by B. C. Giessen (Plenum, New York, 1969), p. 65.
[8] G. Kreiner and H. F. Franzen, J. Alloys Compd. **261**, 83 (1997).
[9] F. J. Edler, V. Gramlich, and W. Steurer, J. Alloys Compd. **269**, 7 (1998).
[10] R. Cerny, M. Francois, K. Yvon, D. Jaccard, E. Walker, V. Petricek, I. Cisarova, H.-U. Nissen, and R. Weissiken, J. Phys.: Condens. Matter **8**, 4485 (1996).
[11] See, e.g., C. Janot, *Quasicrystals*, 2nd ed. (Clarendon, Oxford, 1994), p. 112.
[12] M. Feuerbacher, C. Thomas, and K. Urban, in *Quasicrystals, Structure and Physical Properties*, edited by H.-R. Trebin (Wiley-VCH, Weinheim, 2003), p. 2.
[13] P. C. Gibbons and K. F. Kelton, in *Physical Properties of Quasicrystals*, Springer Series in Solid-State Sciences, Vol. 126, edited by Z. M. Stadnik (Springer, Berlin, 1999), p. 415.
[14] Y. Matsuo and K. Hiraga, Philos. Mag. Lett. **70**, 155 (1994).
[15] M. Yurechko, A. Fattah, T. Velikanova, and B. Grushko. J. Alloys Compd. **329**, 173 (2001).
[16] M. Boudard, H. Klein, M. de Boissieu, M. Audier, and H. Vincent, Philos. Mag. A **74**, 939 (1996).
[17] H. Klein, M. Audier, M. Boudard, M. de Boissieu, L. Behara, and M. Duneau, Philos. Mag. A **73**, 309 (1996).
[18] S. Balanetskyy, B. Grushko, T. Ya. Velikanova, and K. Urban, J. Alloys Compd. **376**, 158 (2004).
[19] M. Yurechko, B. Grushko, T. Velikanova, and K. Urban, J. Alloys Compd. **337**, 172 (2002).
[20] S. Balanetskyy, B. Grushko, and T. Ya. Velikanova, Z. Kristallogr. **219**, 548 (2004).
[21] C. A. Swenson, I. R. Fisher, N. E. Anderson, Jr., P. C. Canfield, and A. Migliori, Phys. Rev. B **65**, 184206 (2002).
[22] L. Beraha, M. Duneau, H. Klein, and M. Audier, Philos. Mag. A **76**, 587 (1997).
[23] H. Klein, M. Feuerbacher, P. Schall, and K. Urban, Philos. Mag. Lett. **80**, 11 (2000).
[24] M. Feuerbacher, H. Klein, and K. Urban, Philos. Mag. Lett. **81**, 639 (2001).
[25] F. E. Mabbs and D. J. Machin, *Magnetism and Transition Metal Complexes* (Chapman and Hall, London, 1973).
[26] F. E. Mabbs and D. J. Machin, Ref. 25, p. 7.
[27] F. Hippert, M. Audier, J. J. Préjean, A. Sulpice, E. Lhotel, V. Simonet, and Y. Calvayrac, Phys. Rev. B **68**, 134402 (2003).
[28] M. Klanjšek, P. Jeglič, P. McGuiness, M. Feuerbacher, E. S. Zijlstra, J. M. Dubois, and J. Dolinšek, Phys. Rev. B **68**, 134210 (2003).
[29] M. Scheffer and J.-B. Suck, Mater. Sci. Eng., A **294–296**, 629 (2000).
[30] V. Simonet, F. Hippert, M. Audier, and Y. Calvayrac, Mater. Sci. Eng., A **294–296**, 625 (2000).
[31] Ž. Bihar, A. Bilušić, J. Lukatela, A. Smontara, P. Jeglič, P. McGuiness, J. Dolinšek, Z. Jagličić, J. Janovec, V. Demange, and J. M. Dubois, J. Alloys Compd. (accepted, 2005).
[32] P. Lanco, T. Klein, C. Berger, F. Cyrot-Lackmann, G. Fourcaudot, and A. Sulpice, Europhys. Lett. **18**, 227 (1992).
[33] H. Akiyama, T. Hashimoto, T. Shibuya, K. Edagawa, and S. Takeuchi, J. Phys. Soc. Jpn. **62**, 939 (1993).
[34] M. Rodmar, B. Grushko, N. Tamura, K. Urban, and Ö. Rapp, Phys. Rev. B **60**, 7208 (1999).
[35] R. Escudero, J. Lasjaunias, Y. Calvayrac, and M. Boudard, J. Phys.: Condens. Matter **11**, 383 (1999).

[36] T. Klein, C. Berger, D. Mayou, and F. Cyrot-Lackmann, Phys. Rev. Lett. **66**, 2907 (1991).
[37] H. Fukuyama and K. Hoshino, J. Phys. Soc. Jpn. **50**, 2131 (1981).
[38] J. Dolinšek, M. Klanjšek, Z. Jagličić, A. Bilušić, and A. Smontara, J. Phys.: Condens. Matter **14**, 6975 (2002).
[39] C. V. Landauro and H. Solbrig, Physica B **301**, 267 (2001).
[40] C. V. Landauro, E. Maciá, and H. Solbrig, Phys. Rev. B **67**, 184206 (2003).
[41] H. Solbrig and C. V. Landauro, in *Quasicrystals, Structure and Physical Properties*, edited by H. R. Trebin (Wiley-VCH, Weinheim, 2003), p. 254.
[42] P. Häussler, R. Haberkern, C. Madel, J. Barzola-Quiquia, and M. Lang, J. Alloys Compd. **342**, 228 (2002).
[43] J. Hafner and M. Krajčí, Phys. Rev. Lett. **68**, 2321 (1992).
[44] J. Hafner and M. Krajčí, Phys. Rev. B **47**, 11795 (1993).
[45] M. Windisch, M. Krajčí, and J. Hafner, J. Phys.: Condens. Matter **6**, 6977 (1994).
[46] J. P. A. Makongo, Y. Moguilnikov, C. Kudla, D. Grüner, M. Schäpers, and G. Kreiner, *Mat. Res. Soc. Symp. Proc.* edited by E. Belin-Ferré, M. Feuerbacher, Y. Ishii, and D. J. Sordelet (Materials Research Society, Warrendale, 2004), Vol. 805, p. 61.
[47] R. Kubo, J. Phys. Soc. Jpn. **12**, 570 (1957).
[48] D. A. Greenwood, Proc. Phys. Soc. London **71**, 585 (1958).
[49] A. Bilušić, Ž Budrović, A. Smontara, J. Dolinšek, P. C. Canfield, and I. R. Fisher, J. Alloys Compd. **342**, 413 (2002).
[50] A. Bilušić, A. Smontara, J. Dolinšek, H. R. Ott, I. R. Fisher, and P. C. Canfield (unpublished).
[51] R. Berman, *Thermal Conduction in Solids* (Oxford University Press, New York, 1978).
[52] P. G. Klemens, *Solid State Physics: Advances in Research and Applications* (Academic Press, New York, 1958), Vol. 7, p. 1.
[53] P. A. Kalugin, M. A. Chernikov, A. Bianchi, and H. R. Ott, Phys. Rev. B **53**, 14145 (1996).
[54] C. Wälti, E. Felder, M. A. Chernikov, H. R. Ott, M. de Boissieu, and C. Janot, Phys. Rev. B **57**, 10504 (1998).
[55] Y. Amazit, M. de Boissieu, and A. Zarembowitch, Europhys. Lett. **20**, 703 (1992).
[56] See, e.g., N. W. Aschroft and N. D. Mermin, *Solid State Physics* (Saunders College, Philadelphia, 1976), p. 505.
[57] C. Janot, A. Magerl, B. Frick, and M. de Boissieu, Phys. Rev. Lett. **71**, 871 (1993).
[58] M. de Boissieu, M. Boudard, R. Bellisent, M. Quilichini, B. Henion, R. Currat, A. I. Goldman, and C. Janot, J. Phys.: Condens. Matter **5**, 4945 (1993).
[59] M. Boudard, M. de Boissieu, S. Kycia, A. I. Goldman, B. Hennion, R. Bellisent, M. Quilichini, R. Currat, and C. Janot, J. Phys.: Condens. Matter **7**, 7299 (1995).
[60] M. Krisch, R. A. Brand, M. Chernikov, and H. R. Ott, Phys. Rev. B **65**, 134201 (2002).
[61] S. Legault, B. Ellman, J. Ström-Olsen, L. Taillefer, T. Lograsso, and D. Delaney, *Quasicrystals, Proceedings of the 6th International Conference, Tokyo, Japan, 1997* (World Scientific, Singapore, 1998), p. 475.
[62] K. Giannò, A. V. Sologubenko, M. A. Chernikov, H. R. Ott, I. R. Fisher, and P. C. Canfield, Phys. Rev. B **62**, 292 (2000).
[63] M. Matsukawa, M. Yoshizawa, K. Noto, Y. Yokoyama, and A. Inoue, Physica B **263-264**, 146 (1999).
[64] N. F. Mott and H. A. Jones, *The Theory of the Properties of Metals and Alloys* (Clarendon, Oxford, 1936).
[65] R. D. Barnard, *Thermoelectricity in Metals and Alloys* (Taylor and Francis, London, 1972), p. 91.